AAS 21-743

CHARACTERISTICS AND ANALYSIS OF FAMILIES OF LOW-ENERGY BALLISTIC LUNAR TRANSFERS

Stephen T. Scheuerle[*], and Kathleen C. Howell[†]

Low-energy ballistic lunar transfers offer propellant efficient paths to the Moon in exchange for longer duration flights. These trajectories rely on the gravitational influence of the Sun to reduce maneuvers at lunar orbit insertion. Due to the sensitive nature of transfers navigating between cislunar and heliocentric space, developing ballistic lunar transfers that fulfill mission-specific constraints remains a challenge. An Earth-Moon-Sun four-body model, i.e., the bicircular restricted four-body problem (BCR4BP), is incorporated to construct end-to-end ballistic lunar transfers. Families of transfers with both fixed trans-lunar injection and lunar orbit insertion maneuver costs are examined. A methodology to assess the sensitivity of ballistic lunar transfers is evaluated to aid in expanding the launch window for these epoch dependent paths.

INTRODUCTION

As spacecraft technology continues to develop, and the demand for missions to cislunar space increases, further low-energy trajectory analysis is necessary to assess viable transfer options. NASA aims to develop a sustainable presence in cislunar space through the development of the Artemis and Gateway programs, and in collaboration with private industry.[1] For a given mission, the spacecraft hardware characteristics influence available paths to the Moon. For missions where the time of flight is flexible, low-energy transfers offer propellant efficient paths to the lunar region. A group of low-energy transfers, i.e., ballistic lunar transfers, leverage solar perturbations by spending multiple months beyond the orbit of the Moon. Multiple spacecraft in the near-future with limited propulsion capabilities, plan to leverage ballistic lunar transfers to reach cislunar space, including NASA's Cislunar Autonomous Positioning System Technology Operations and Navigation Experiment (CAPSTONE)[2] and JAXA's Equilibrium Lunar-Earth point 6U Spacecraft (EQUULEUS).[3] This analysis leverages techniques in dynamical systems theory within the Bicircular Restricted-Four Body Problem (BCR4BP) to construct families of ballistic lunar transfers. The families are designed to offer a range of solutions for given spacecraft constraints, i.e. arrival epoch at the Moon, insertion maneuver magnitude, and flyby capabilities.

DYNAMICAL MODELS

Two models are employed in this investigation to represent the motion of a ballistic lunar transfer. The Circular Restricted Three-Body Problem (CR3BP) is a gravity model that describes the

[*]Ph.D. Student, School of Aeronautics and Astronautics, Purdue University, West Lafayette, IN 47907; sscheuer@purdue.edu

[†]Hsu Lo Distinguished Professor, School of Aeronautics and Astronautics, Purdue University, West Lafayette, IN 47907; howell@purdue.edu. Fellow AAS; Fellow AIAA

motion of a spacecraft in the vicinity of two, gravitationally massive bodies. Properties of the differential equations in the CR3BP aid in the classification and characterization of motion throughout the system, and yields initial guesses for transitioning into higher fidelity models. The Bicircular Restricted Four-Body Problem (BCR4BP) depicts the motion of a spacecraft relative to a planet-moon-star system. The BCR4BP is a key framework in this analysis, as the nature of ballistic lunar transfer relies on the cumulative influence of the Earth, Moon, and Sun. The investigation leverages properties and dynamical structures from both models to construct ballistic lunar transfers.

Circular Restricted Three-Body Problem

Ballistic lunar transfers depart the Earth, reach distances significantly beyond the lunar orbit and ultimately arrive into the vicinity of the Moon. Periodic motion in the CR3BP offers insight into the structures upon arrival near the Moon. The CR3BP describes the motion of a massless particle (P_3) due to the gravitational field of two massive bodies (P_1 and P_2). The CR3BP is incorporated such that Earth is P_1 and the Moon is P_2, where the mass of the bodies are M_1 and M_2, respectively. The model assumes the Earth and the Moon move in circular orbits about their mutual barycenter B_1. By formulating the equations of motion in a coordinate frame that rotates with the primary bodies, the differential equations are time-independent.[4] The equations of motion in the CR3BP are nondimensionalized to reduce errors with numerical propagation. The three scalar nonlinear second-order differential equations that describe the motion of particle P_3 in the rotating frame are,

$$\ddot{x} = 2\dot{y} + \frac{\partial U}{\partial x} \qquad \text{(1a)} \qquad \ddot{y} = -2\dot{x} + \frac{\partial U}{\partial y} \qquad \text{(1b)} \qquad \ddot{z} = \frac{\partial U}{\partial z} \qquad \text{(1c)}$$

where x, y, z and $\dot{x}$, $\dot{y}$, $\dot{z}$ are the position and velocity components of P_3. The variable μ is the mass parameter, defined $\mu = \frac{M_2}{M_1+M_2}$. For the Earth-Moon system, $\mu \approx 0.01215$. The terms $\frac{\partial U}{\partial x}$, $\frac{\partial U}{\partial y}$, and $\frac{\partial U}{\partial z}$ are the partial derivatives of the pseudo potential function U with respect to the position of P_3. The pseudo-potential function, U, is written as,

$$U = \frac{1}{2}\left(x^2 + y^2\right) + \frac{1-\mu}{r_{13}} + \frac{\mu}{r_{23}} \tag{2}$$

where r_{ij} is the scalar distance between body i and j. The CR3BP possess five equilibrium solutions denoted the Lagrange point and represented as L_1 through L_5. There is no closed-form solution for the equations of motion in the CR3BP, however, a single integral of the motion exists. The integral of the motion is denoted the Jacobi Constant value (C), and written as,

$$C = 2U - (\dot{x}^2 + \dot{y}^2 + \dot{z}^2) \tag{3}$$

Equation (3) illustrates that an increase in the velocity of P_3 corresponds to a value of C that decreases. Thus, an increase in the value of the Jacobi Constant reflects a decrease in the energy of P_3 relative to the Earth-Moon system.

Characteristics of the differential equations in the CR3BP aid in trajectory design within a multi-body dynamical regime. The Jacobi Constant value yields insight into the energy of a spacecraft, an approximation for a theoretical minimum maneuver cost, and the accessibility of various regions throughout cislunar space. As the equations of motion lack a term that is explicitly dependent on time, the motion of P_3 is strictly a function of the position and velocity in the rotating coordinate frame. Such a time-independent model is advantageous to assess periodic motion. The inclusion of the CR3BP in this investigation is to transition periodic orbits to the BCR4BP.

Bicircular Restricted Four-Body Problem

The BCR4BP is the primary dynamical model incorporated in this analysis. The BCR4BP describes the motion of a massless particle (P_3) due to the gravitational field of three massive bodies (P_1, P_2, and P_4). The BCR4BP effectively models the motion of a planet-moon-star system. The Earth and Moon are P_1 and P_2, respectively. The Sun is represented as the massive primary, P_4. The motion of the Earth and Moon are assumed to move in circular orbits about their common barycenter (B_1), similar to the assumptions in the CR3BP. The Sun and the Earth-Moon system are assumed to be in circular orbits about the total system barycenter (B_2). The orientation of the Sun relative to the Earth-Moon rotating frame is defined in terms of the Sun angle (θ_S), and is illustrated in Figure 1. The term a_S is the scalar distance between the Sun and Earth-Moon barycenter B_1. The Sun traverses in the clockwise direction relative to B_1 in the Earth-Moon rotating frame. In the

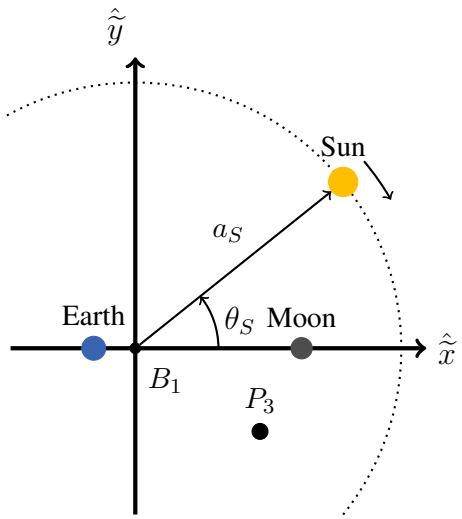

Figure 1. The Earth-Moon rotating coordinate frame in the BCR4BP

full Earth-Moon-Sun system, the orbital path of the Moon does not lie in the ecliptic plane, i.e., the motion of the Sun relative to the Earth and Moon is three-dimensional. The BCR4BP model incorporated in this analysis assumes the Earth, Moon, and Sun are coplanar throughout time. Although the coplanar assumption is not representative of the true motion of the bodies, it is adequate for this analysis. It is advantageous to represent the motion of the spacecraft in both the Earth-Moon and Sun-B_1 rotating frames. To distinguish between the two frames, quantities in the Earth-Moon rotating frame are defined with tildes, and values in the Sun-B_1 rotating frame are underlined. The equations of motion for P_3 in the BCR4BP are formulated relative to the Earth-Moon rotating frame, as

$$\ddot{\tilde{x}} = 2\dot{\tilde{y}} + \frac{\partial \Upsilon}{\partial \tilde{x}} \qquad (4a) \qquad \ddot{\tilde{y}} = -2\dot{\tilde{x}} + \frac{\partial \Upsilon}{\partial \tilde{y}} \qquad (4b) \qquad \ddot{\tilde{z}} = \frac{\partial \Upsilon}{\partial \tilde{z}} \qquad (4c)$$

where Υ is the pseudo-potential function for the differential equations in the BCR4BP as represented in the Earth-Moon rotating frame. The pseudo-potential function is expressed in terms of the orientation of the Sun in the rotating frame, and written as

$$\Upsilon = \frac{1}{2}\left(\tilde{x}^2 + \tilde{y}^2\right) + \frac{1-\mu}{r_{13}} + \frac{\mu}{r_{23}} + \frac{m_4}{r_{43}} - \frac{m_4}{a_S^2}\left(\tilde{x}\cos(\theta_S) + \tilde{y}\sin(\theta_S)\right) \qquad (5)$$

where μ is the mass parameter of the Earth-Moon system, m_4 is the nondimensional mass of the Sun, i.e. $m_4 = \frac{M_4}{M_1+M_2}$. Recall that a_S is the constant distance from the Sun to the Earth-Moon barycenter, B_1, and θ_S is the angle that orients the Sun in the Earth-Moon rotating frame. Although the model is time-dependent, the assumptions yield a periodic model that describes the motion of a spacecraft under the gravitational influence of three massive bodies. The differential equations in the BCR4BP yield two 'energy-like' quantities similar to the Jacobi Constant value, denoted the Earth-Moon and Sun-B_1 Hamiltonian.[5] In contrast to the Jacobi Constant, the Hamiltonian values are not integrals of the motion, and vary as the spacecraft evolves through the model. The Earth-Moon Hamiltonian is expressed,

$$H_{EM} = 2\Upsilon - (\dot{\tilde{x}}^2 + \dot{\tilde{y}}^2 + \dot{\tilde{z}}^2) \tag{6}$$

Variations in the Earth-Moon and Sun-B_1 Hamiltonians offer insight into the natural evolution of the energy due to Solar and Earth-Moon perturbations, respectively.[6] The differential equations in the BCR4BP do not deliver equilibrium solutions, as the model evolves with time. However, for a fixed epoch, constant instantaneous equilibrium locations can be computed. As ballistic lunar transfers depend on the gravitational influence of all three primary bodies, the BCR4BP is an effective approach to modeling end-to-end paths.

NEAR RECTILINEAR HALO ORBITS

To develop families of ballistic lunar transfers, various lunar destination orbits are available. Previous authors have investigated paths to target locations around the Moon. Parker and Born explored trajectories to multi-body unstable orbits through the use of a coupled CR3BP model.[7] McCarthy and Howell examined the use of quasi-periodic orbit manifolds to construct ballistic lunar transfers.[8] This investigation considers paths to planar low lunar orbits (LLO) as well as the NASA Gateway southern L_2 NRHO.

Gateway is an orbital platform being developed by NASA to offer an infrastructure for both scientific and crewed exploration about the Moon.[9] The intended orbit for Gateway is a southern L_2 Near Rectilinear Halo Orbit (NRHO), offering constant communications with Earth, and extended coverage over the Moon's south pole. The NRHOs are a subset of the L_1 and L_2 halo families in the CR3BP. In the Earth-Moon system, the NRHO families are nearly-stable, offering an effective location for long-term habitats in cislunar space.[10] Although the nearly-stable behaviour offers an effective staging ground for stationkeeping, designing low-energy transfers and inserting into an NRHO is nontrivial. As the Gateway program continues design and development, there is an increasing demand in options for accessing the NRHO from Earth. The specific orbit incorporated into this analysis is the southern L_2 9:2 synodic resonant NRHO. The values 9:2 represent the resonance ratio between the orbital period and synodic period of the Earth-Moon system. An illustration of the southern L_2 9:2 synodic resonant NRHO in represented in Figure 2 as computed in the CR3BP. The blue curve is the periodic orbit with a period of approximately six and a half days. The gray sphere approximates the size of the Moon as a sphere is constant radius 1737 km.

Multiple southern L_2 9:2 synodic resonant NRHOs exist in the BCR4BP. A difference between the CR3BP and the BCR4BP is the inherent time dependency of the four-body model. Relative to the Earth-Moon rotating frame, the motion of the spacecraft relies on the position, velocity, and relative orientation to the Sun, i.e., the Sun angle. When transitioning a periodic orbit between the CR3BP and the BCR4BP, an initial Sun angle must be added to the state vector.[6] Computing periodic orbits in the BCR4BP is nontrivial, as solar perturbations may impact the geometry and

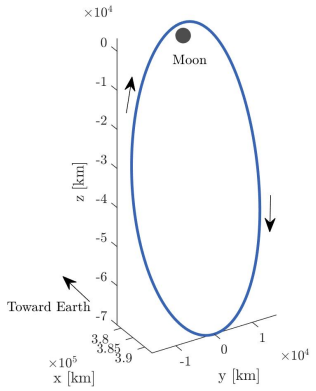

Figure 2. Southern L_2 9:2 synodic resonant NRHO in the Earth-Moon CR3BP, illustrated in the Earth-Moon rotating frame

stability of the orbit. Likewise, it is not guaranteed that an orbit with a synodic resonance that exists in the CR3BP will also exist in the BCR4BP. Boudad et al. applied a Sun mass continuation scheme to compute multiple NRHOs in the BCR4BP.[11] As ballistic lunar transfers are sensitive to slight changes in epoch, arriving at different of 9:2 NRHOs in the BCR4BP offers a wider range of solutions.

A multi-dimensional Newton-Raphson scheme is employed to construct a family of southern L_2 9:2 synodic resonant NRHOs in the BCR4BP. Previous investigations detail techniques to compute periodic orbits in the BCR4BP through perpendicular crossing techniques.[6] The perpendicular crossing method requires the velocity of the spacecraft to be perpendicular to the radial direction of each primary body at two instances in time. In the planar BCR4BP, such a condition is epoch dependent, i.e., when the Sun angle is equivalent to an integer multiple of π. Using the periodic orbit from the CR3BP, and leveraging the perpendicular crossings, a southern L_2 9:2 synodic resonant NRHO is constructed in the BCR4BP, as illustrated in Figure 3(a). The blue curve is one continuous, closed curve repeating after 9 revolutions about the Moon. The period of the entire orbit is two synodic months. Comparing Figure 2 to Figure 3(a) demonstrates the influence of the Sun on the orbit, as the spacecraft position at apolune varies across the nine different revolutions. At each instance along the orbit where the Sun angle is equal to an integer multiple of 2π, a perpendicular crossing exists. The same periodic orbit is represented in the Sun-B_1 rotating frame, and appears in Figure 3(b). The Earth and Moon move in the Sun-B_1 rotating frame as the position of the Sun remains fixed. The motion of the Earth is the green circle near the origin, and the Moon's orbit is the dark gray circle. The blue curve is the same southern L_2 9:2 synodic resonant NRHO as illustrated in Figure 3(a), now following the path of the Moon as the system rotates about the barycenter B_1. The motion of the orbit relative to the Sun is more clearly apparent in the Sun-B_1 rotating frame. The orientation of this specific NRHO in the BCR4BP has advantages in-terms of Earth-eclipse avoidance.[11] Consider the initial epoch to be the $\underline{xz}$-plane crossing above the Moon. For this particular solution, such conditions represent a Sun angle of zero degrees. To construct a family of 9:2 synodic resonant NRHOs in the BCR4BP, a natural parameter continuation scheme is applied. The method includes six free variables, i.e., the initial position and velocity components of the orbit. Due to the definition of a periodic orbit in the BCR4BP, the period must an integer multiple of the synodic period to secure resonance in the Earth-Moon-Sun system. For the 9:2 NRHO,

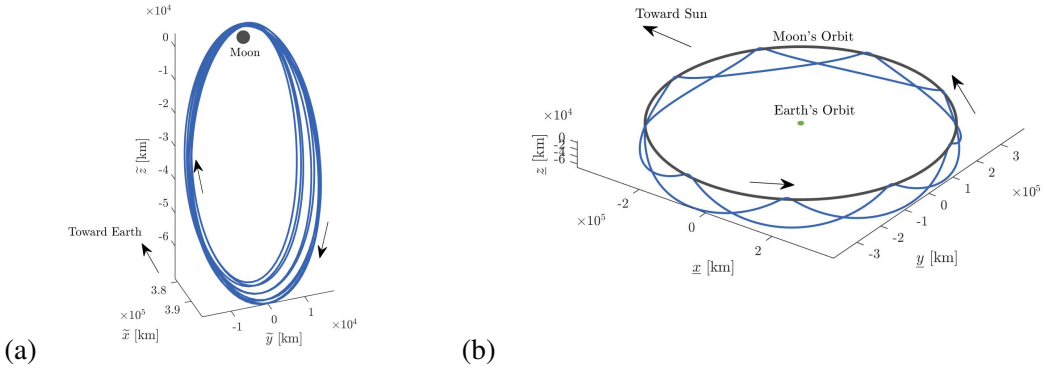

(a) (b)

Figure 3. The perpendicular crossing southern L_2 9:2 synodic resonant NRHO in the Earth-Moon-Sun BCR4BP, illustrated in the Earth-Moon rotating frame (a) and the Sun-B_1 rotating frame (b)

after two synodic months, the final position and velocity components for the transfer must return to the initial state vector. For the current formulation, the number of free variables matches the number of constraints, i.e., the Jacobian is non-singular. However, by continuing the initial orbit in Sun angle, there is no constraint that restricts the state from simply returning the current solution in the numerical process. To avoid reconverging on the previous solution, an additional constraint is added, such that the initial state lies on the $\widetilde{x}\widetilde{z}$-plane, i.e., $\widetilde{y}_i = 0$. Therefore, the free variables are reduced to

$$\bar{X} = \begin{bmatrix} \widetilde{x}_i & \widetilde{z}_i & \dot{\widetilde{x}}_i & \dot{\widetilde{y}}_i & \dot{\widetilde{z}}_i \end{bmatrix} \tag{7}$$

where $\bar{X}$ is the free variable vector, and the quantities with subscript i comprise the initial state along the orbit. The periodicity constraint is then represented as

$$\bar{F} = \begin{bmatrix} \widetilde{x}_f - \widetilde{x}_i & \widetilde{y}_f & \widetilde{z}_f - \widetilde{z}_i & \dot{\widetilde{x}}_f - \dot{\widetilde{x}}_i & \dot{\widetilde{y}}_f - \dot{\widetilde{y}}_i & \dot{\widetilde{z}}_f - \dot{\widetilde{z}}_i \end{bmatrix} \tag{8}$$

where $\bar{F}$ is the constraint vector and the quantities with subscript f are the final state along the orbit, after propagation for two synodic months. As there are more constraints than free variables, the Jacobian is overdetermined. The propagation time is long and requires nine passes in close proximity of the Moon, thus, a multiple shooting technique is employed to aid in the convergence process. The least-squares approximation is applied to locate solutions within the convergence basin. The procedure yields a family of 9:2 synodic resonant NRHOs in the BCR4BP for each initial Sun angle; they are periodic to within 10 m in position and 2 mm/sec in velocity. The family of periodic orbits in the Earth-Moon rotating frame is represented in Figure 4. A subset of ten orbits from the family are included in the figure. Note that the difference in many of these solutions relies on the solar epoch epoch, thus, it is hard to discern different periodic solutions as they exist in similar position-space. The difference in the members of the family are more apparent in the Sun-B_1 frame, as illustrated in Figure 5. The same subset of ten orbits are represented in both Figure 4 and Figure 5, with the only difference a view in the rotating coordinate frame. As the family of 9:2 NRHOs in the BCR4BP are evolving across initial Sun angle, the initial $\widetilde{x}\widetilde{z}$-plane crossing, i.e., position above the Moon, is epoch dependent. Comparing Figure 3(b) to Figure 5, the range of

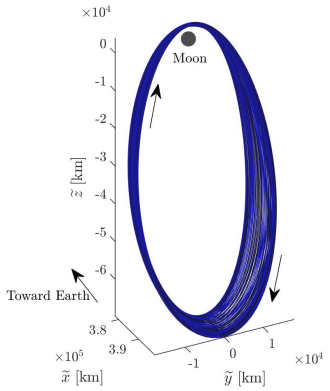

Figure 4. Family of southern L_2 9:2 synodic resonant NRHOs in the BCR4BP, expressed in the Earth-Moon rotating frame

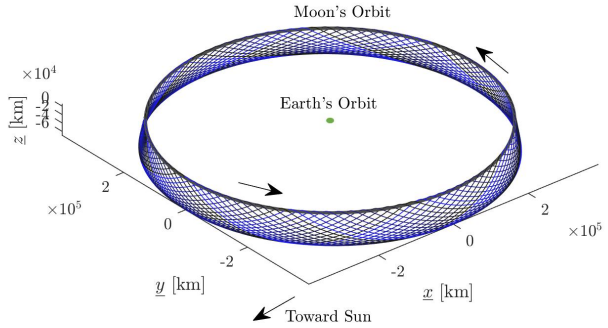

Figure 5. Family of southern L_2 9:2 synodic resonant NRHOs in the BCR4BP, illustrated in the Sun-B_1 rotating frame centered at B_1

available orbits along the family relative to the Sun by shifting the initial Sun angle is highlighted. Each member of the family possesses nine perilunes at varying Sun angles. The perilunes are not constrained to the $\widetilde{x}\widetilde{z}$-plane. The perilune radius and the Sun angles are recorded across the family and plotted in Figure 6. As a basis of comparison, the 9:2 NRHO in the CR3BP as a periapse radius of approximately 3,200 km.

BALLISTIC LUNAR TRANSFERS

Ballistic lunar transfers leverage solar perturbations to reduce maneuver costs associated with arriving into the lunar vicinity. Trajectory design typically balances mission criteria with navigational capabilities to yield solutions to arrive at desired destinations in space. A typical trade-study when analyzing transfers comparing flight duration and propellant cost, i.e., ΔV. Low-energy transfers incorporate the underlying dynamical flow of the models to produce solutions with a lower ΔV and, generally, longer flight times. Ballistic lunar transfers are a type of low-energy transfer that, after

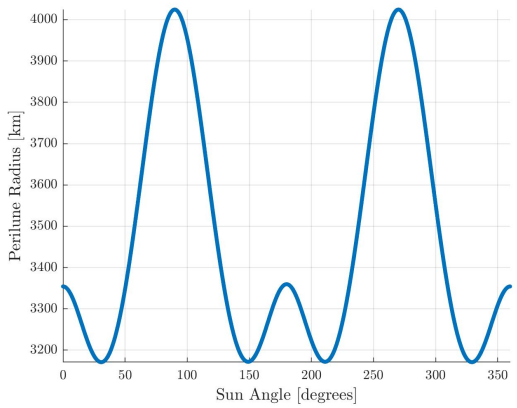

Figure 6. Evolution of perilune radius as a function of Sun angle for the family of southern L_2 9:2 synodic resonant NRHOs in the BCR4BP

Earth departure, evolve out toward the Sun-Earth Lagrange points, then flow back to the lunar region.[12] Ballistic lunar transfers often require flight times of multiple months, typically ranging from 90 to over 120 days. As the trajectories rely on a relative orientation in the Earth-Moon-Sun system, the paths are sensitive to variations in epoch. An ideal ballistic lunar transfer includes only two maneuvers, the trans-lunar injection (TLI) to embark from Earth orbit, and the lunar orbit insertion (LOI) to arrive into the cislunar orbit. This investigation considers two properties of ballistic lunar transfers. First, the inherent design of the end-to-end transfer, leveraging properties of the multi-body dynamical regime to reduce the cost of both TLI and LOI. Secondly, introducing techniques to aid in the design of a ballistic lunar transfer by extending launch window options.

Initial Guess Generation

Various techniques in dynamical systems theory offer strategies for identifying an initial guess. For transfers to multi-body periodic orbits, Poincaré sections reduce the complexity of the solution-space and supply some clarity in representing desirable paths. For ballistic lunar transfers, a specific example pf an insightful type of map in this problem is a periapse Poincaré map. Previous authors leverage periapse Poincaré maps to characterize the behavior of a spacecraft or to seed initial guesses for different types of transfers.[8,13,14] Consider a sample scenario formulated to deliver a spacecraft from Earth to a 9:2 synodic resonant NRHO. The periodic solution from Figure 3(a) is selected to represent transfers that arrive at a distinct epoch, i.e, phasing condition. The Poincaré map for this scenario is constructed by discretizing the desired arrival orbit, applying an impulsive maneuvers at each point, and propagating in reverse time to yield instances where perigees occur.[8] Given a 15 m/sec maneuver in the rotating velocity direction at ten thousand points along the 9:2 NRHO in the BCR4BP, and a maximum transfer duration of one year, a periapse map projected onto the $\hat{\tilde{x}}\hat{\tilde{y}}$-plane is illustrated in Figure 7. Each point marks a perigee, i.e., closest approach to Earth in negative time, and the color of the dot designates the transfer time from the perigee state to insertion into the NRHO at the departure location. The green circle is an approximate representation of the Earth (sphere with radius 6378 km), and the black circle is a 150 km altitude, planar, low Earth orbit (LEO). Although the perigee locations are spatial, the predominant displacement from Earth lie in the $\tilde{x}\tilde{y}$-plane. Note that the periodic NRHO employed to construct Figure 7 is epoch specific, i.e., the initial perilune is defined for a Sun angle equal to zero degrees. By selecting a different

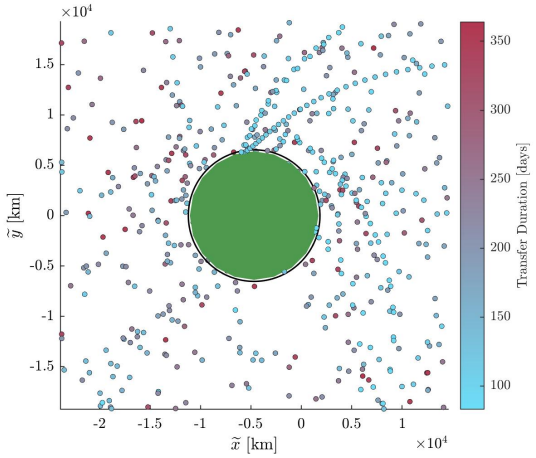

Figure 7. Periapse Poincaré map for 9:2 NRHO with initial perilune at 0 degrees projected onto the $\widetilde{x}\widetilde{y}$-plane, BCR4BP Earth-Moon rotating frame

9:2 NRHO from the family determined previously, an entirely new map results. For a southern L_2 9:2 NRHO with an initial perilune at 10 degrees, the periapse map in Figure 8 is constructed. Comparing the two maps indicate ballistic lunar transfers that depart at different locations relative to the Earth-Moon system. A periapse with a time of flight of 100 days is selected from Figure 7.

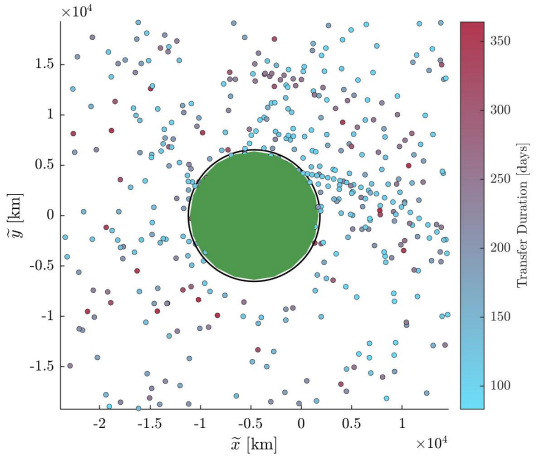

Figure 8. Periapse Poincaré map for 9:2 NRHO with initial perilune at 10 degrees projected onto the $\widetilde{x}\widetilde{y}$-plane, BCR4BP Earth-Moon rotating frame

The transfer departs from a 150 km altitude LEO and traverses beyond the orbit of the Moon before insertion into the NRHO, with a lunar orbit insertion cost (ΔV_{LOI}) of 15 m/sec. The sample transfer in the Sun-B_1 rotating frame is depicted in Figure 9. The black circle is the lunar orbit, $\underline{L}_1$ and $\underline{L}_2$ are the locations of the Lagrange points for the Sun-B_1 CR3BP.[6] The spatial ballistic lunar transfer is the blue arc projected onto the $\underline{\hat{x}}\underline{\hat{y}}$-axis. The same transfer is illustrated in the Earth-Moon rotating frame in Figure 10(a) and Figure 10(b). A $\widetilde{x}\widetilde{y}$-plane projection of the entire transfer from the Earth to the NRHO is plotted in Figure 10(a). Ballistic lunar transfers appear to encircle the Earth-Moon system as the transfer path is propagated over multiple months beyond lunar orbit. A representation of the spatial motion upon arrival near the Moon appears in Figure 10(b). The yellow curve is the

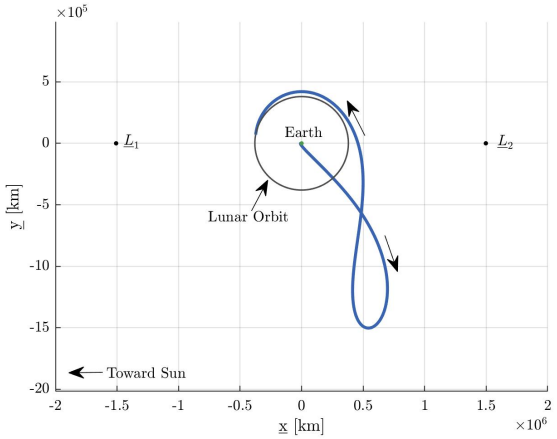

Figure 9. Planar projection of a ballistic lunar transfer to a 9:2 NRHO with a ΔV_{LOI} = 15 m/sec, Sun-B_1 rotating frame centered at B_1

arrival NRHO, and the gray sphere is the Moon, all constructed in the BCR4BP.

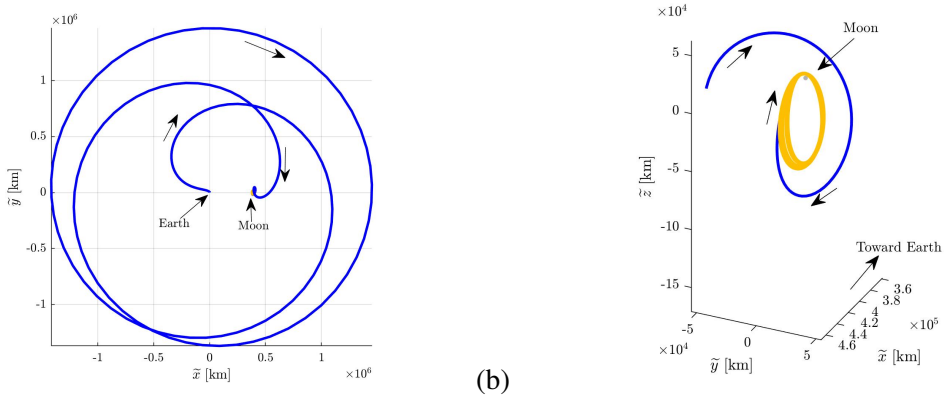

Figure 10. Ballistic lunar transfer to a 9:2 NRHO, planar projection (a) and spatial arrival (b) in the Earth-Moon rotating frame

Families Constructed for Fixed Maneuvers

Families that are determined via fixed values for a maneuver characterize the types of ballistic lunar transfers available for a given mission criteria. As ballistic lunar transfers inherently rely on TLI and LOI, two fixed maneuver families exist. A fixed TLI maneuver magnitude family considers the range of ballistic lunar transfer available for a given injection maneuver from Earth. It is common for TLI maneuver to be delivered by the launch vehicles. A fixed TLI maneuver family demonstrates the geometries available for a given launch which the fixed TLI constraint, F_{TLI}, is evaluated as,

$$F_{\text{TLI}} = \sqrt{\dot{\tilde{x}}_0^2 + \dot{\tilde{y}}_0^2 + \dot{\tilde{z}}_0^2} - \Delta V_{\text{TLI}} - V_{\text{LEO}} \tag{9}$$

where the terms with a subscript zero are the initial velocity components of the transfer, ΔV_{TLI} is the maneuver magnitude of the TLI maneuver, and V_{LEO} is the orbital velocity of the parking orbit. A sample ballistic lunar transfer from a 150 km altitude LEO to a 100 km altitude LLO is illustrated in Figure 11. The flight duration is 75 days, and a TLI maneuver magnitude equal to 3.211 km/sec. The gray circle represents the orbit of the Moon in the BCR4BP. Using the ballistic lunar transfer

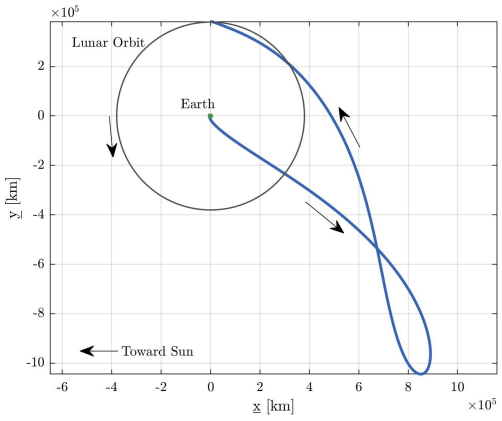

Figure 11. Ballistic lunar transfer to a 100 km circular LLO in the BCR4BP, Sun-B_1 rotating frame centered at B_1

from Figure 11 and the constraint from Equation (9), a family of ballistic lunar transfers with a TLI maneuver magnitude of 3.211 km/sec is constructed. A subsection of the family, all transfers with LOI maneuvers of less than 800 m/sec is plotted in Figure 12(a). The blue curve represents the member of the family plotted with the shortest flight duration, i.e., a time of flight of 64.7 days and a LOI maneuver magnitude of 800 m/sec. The red curve is the ballistic lunar transfer in this family with the lowest LOI cost, corresponding to a time of flight equal to 77.5 days and a LOI maneuver of 667 m/sec. The variation in LOI cost and time of flight is plotted as the yellow line in Figure 12(b). The colored points on Figure 12(b) relate to the color transfers in Figure 12(a).

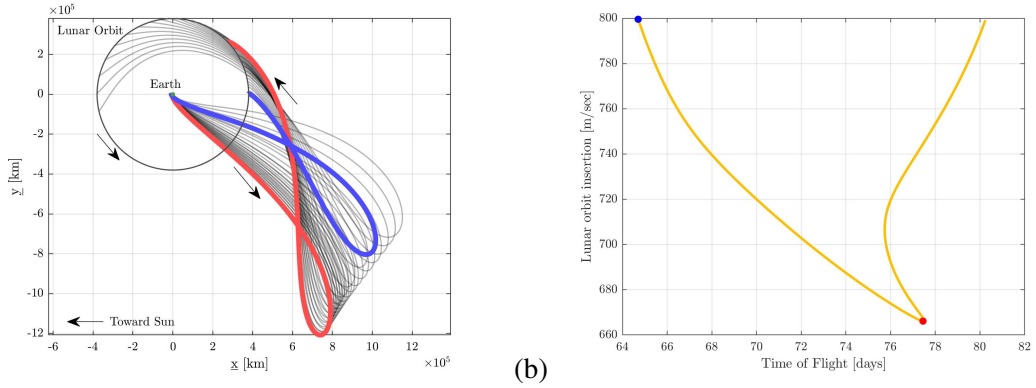

(a) (b)

Figure 12. Family of ballistic lunar transfers with a fixed TLI maneuver of 3.221 km/sec, Sun-B_1 rotating frame centered at B_1 (a) and evolution of LOI and time of flight along the family (b)

Outbound lunar flybys reduce the necessary injection cost required for a ballistic lunar transfer. The previous example illustrated the range of available solutions for a fixed TLI maneuver. A

technique to reduce the injection maneuver cost is to incorporate an outbound lunar flyby. By seeding the problem with an initial guess that leverages a lunar or Earth flyby, and targeting a low TLI maneuver magnitude, the problem implicitly constrains the solutions to leverage a flyby. Consider a ballistic lunar transfer with an outbound lunar flyby as represented in Figure 13. The flyby occurs when the blue trajectory passes the lunar orbit, as there is a close approach of 9,000 km between the spacecraft and the Moon. The time of flight for this transfer is 84 days, and the TLI maneuver cost is 3.153 km/sec. The trajectory from Figure 13 is then seeded as an initial guess for

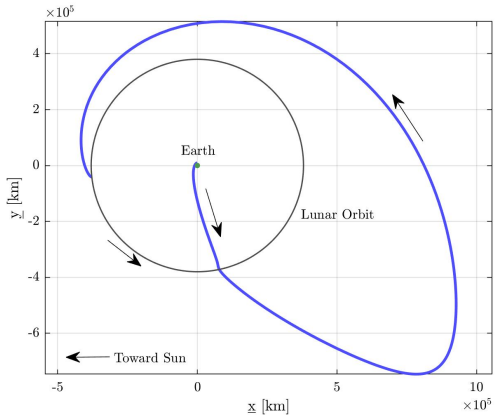

Figure 13. Ballistic lunar transfers with an outbound lunar flyby, Sun-B_1 rotating frame centered at B_1

a family of fixed TLI maneuver transfers. As the injection cost is 3.153 km/sec, the family grows with the implicit constraint that a lunar flyby is necessary. The family of ballistic lunar transfers is plotted in Figure 14(a). Recall that the orbits in the family all originate from a LEO with an altitude of 150 km and arrive in a planar LLO with an altitude of 100 km. The blue curve is the member of the family with the shortest flight duration, i.e., 78.7 days and a LOI cost of 668 m/sec. The red arc is the member of the family with the lowest insertion cost, i.e., 640 m/sec and corresponds to a time of flight that equals 84 days. The initial epoch for the family spans three days, and the arrival epoch at the Moon spans 20 days. The colored points on Figure 14(b) designate the location on the plot for the respective color transfers in Figure 14(a).

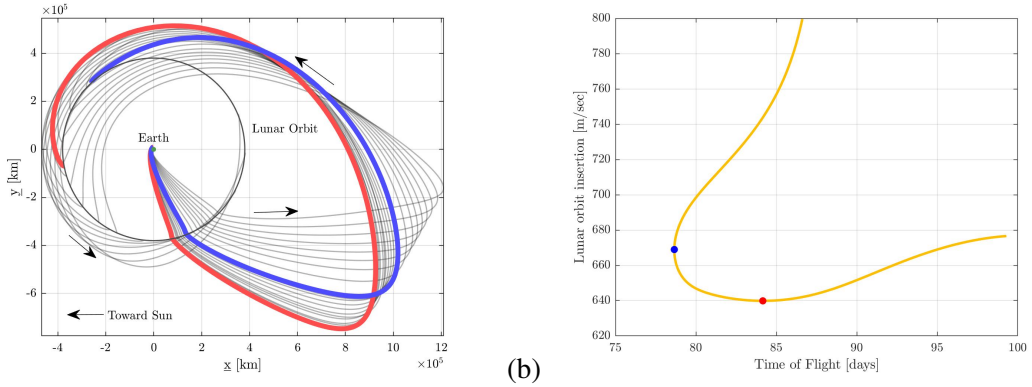

Figure 14. Family of ballistic lunar transfers with an outbound lunar flyby, Sun-B_1 rotating frame centered at B_1 (a) and the variation in LOI costs and time of flight (b)

In contrast to families with fixed TLI maneuvers, families of transfers with a fixed LOI maneuver magnitude classify the geometry for transfers that arrive into the lunar vicinity. As it is common for the TLI injection to depart Earth is delivered by a launch vehicle, the insertion ΔV into a desired orbit about the Moon is carried by the spacecraft. If allowable insertion into lunar orbit is budgeted, characterizing the available geometries for that maneuver magnitude is advantageous. Consider a set of transfers that depart from the parking orbit, and arrive into the desired lunar orbit such that the LOI insertion maneuver is of a fixed magnitude. The constraint to fix the LOI maneuver is written as,

$$F_{\text{LOI}} = \sqrt{\dot{\tilde{x}}_f^2 + \dot{\tilde{y}}_f^2 + \dot{\tilde{z}}_f^2} - \Delta V_{\text{LOI}} - V_{\text{Destination}} \tag{10}$$

where F_{LOI} is the constraint, quantities with subscript f are evaluated at the end of the transfer, and the value ΔV_{LOI} is the fixed LOI cost. The variable $V_{\text{Destination}}$ is defined as the velocity on the destination orbit at the insertion point. To construct a family of transfers such that all the trajectories possess precisely the same LOI maneuver magnitude, a ballistic lunar transfer is initially designed given an instantaneous equilibrium solution as a departure condition. Previous analysis has illustrated that trajectories departing an instantaneous equilibrium points in the BCR4BP offer low-cost transfer designs to the Moon.[6,15] A sample transfer departing an instantaneous equilibrium point is illustrated in Figure 15. The time of flight for the transfer is 138.6 days, a longer flight duration than the previous examples. However, by leveraging the dynamics of the four-body problem, the maneuver cost to insert into the 100 km altitude LLO is 630 m/sec. By employing the Earth-Moon Hamiltonian, the theoretical minimum ΔV required to insert into a planar, 100 km altitude LLO in the BCR4BP is 626.3 m/sec.[6] The trajectory from Figure 15 and the constraint from Equation (10)

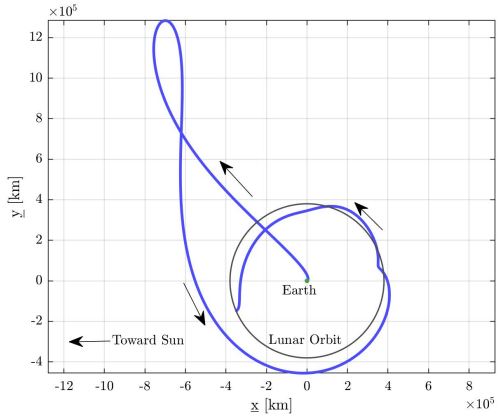

Figure 15. Ballistic lunar transfer off of an instantaneous equilibrium point, Sun-B_1 rotating frame centered at B_1

subsequently produce a family of transfers that depart from a 150 km altitude LEO to a 100 km altitude LLO with a fixed LOI magnitude of 630 m/sec. The range of solutions vary in flight duration, departure and arrival epoch, and the injection cost at Earth departure. The family of ballistic lunar transfers is illustrated as the gray curves in Figure 16(a). The orbit of the Moon is again depicted as the gray circle. The blue arc is the solution with the shortest flight duration, i.e., 103.5 days and with a TLI cost of 3.210 km/sec. The red curve corresponds to the lowest TLI maneuver cost, i.e., 3.142 km/sec and a flight duration of 137.5 days. The available launch window for this family spans 23 days, and is repeatable each synodic period (29.5 days). The variation in TLI cost and time of

flight is plotted in Figure 16(b). The colored points on Figure 16(b) correspond to the respective color transfers in Figure 16(a).

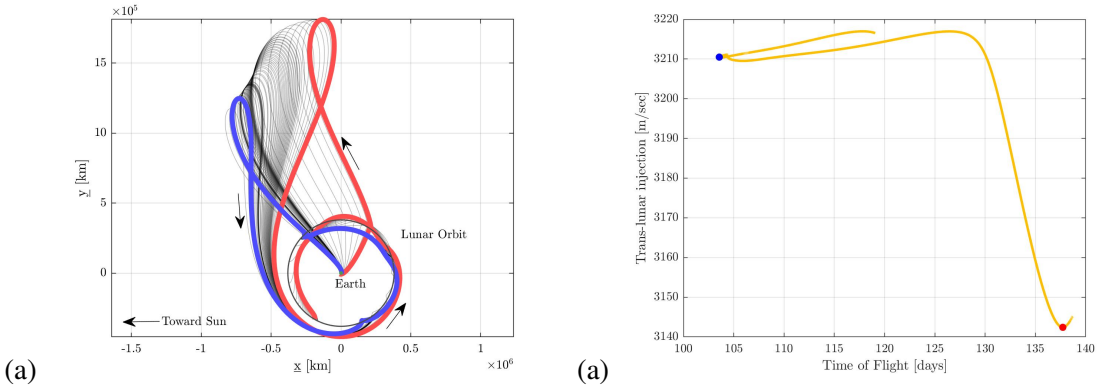

(a) (a)

Figure 16. Family of ballistic lunar transfer with fixed LOI maneuver of 630 m/sec, Sun-B_1 rotating frame centered at B_1 (a) and the evolution of TLI costs and time of flight (b)

Fixed maneuver families provide insight into insertion conditions upon arrival into a multi-body orbit. Thus far, the fixed TLI or LOI maneuver families are always constructed for transfers to a 100 km altitude, planar LLO. However, the constraint is applicable to any desired destination in cislunar space. Recall the previous analysis concerning transfer trajectories to the 9:2 NRHO. Given the ballistic lunar transfer from Figure 9, new families of ballistic lunar transfers are constructed. Members within a family depart from a 150 km altitude LEO and arrives into the same 9:2 NRHO with a fixed LOI cost. Each family is parameterized with a different fixed LOI maneuver magnitude, ranging from 15 m/sec to 50 m/sec. The insertion location along the NRHO is free to vary. The flight duration and insertion Sun angle vary depending on the allotted maneuver magnitude, as illustrated in Figure 17. Each curve represents a different family defined by a specific LOI maneuver value. As position and velocity states in the BCR4BP are epoch dependent, for LOI maneuver values ranging from 15 to 50 m/sec, the insertion Sun angle corresponds to a unique insertion state on the 9:2 NRHO. Therefore, the Sun angles illustrated in Figure 17 relate to specific locations along the NRHO. If it is desired to insert into the NRHO at a specific epoch, i.e., Sun angle, multiple solutions exist with varying time of flight. For example, consider the magenta curve corresponding to a LOI maneuver value of ΔV_{LOI} = 50 m/sec. If the mission is constrained to arrive into the NRHO at a specific location, i.e., corresponding to a Sun angle of 10 degrees, then there are two viable ballistic lunar transfers. Generally, increasing the LOI maneuver magnitude expands the regions along the NRHO that are accessible. The insertion maneuver direction is constrained to the $\hat{\tilde{x}}\hat{\tilde{y}}$-plane.

OPERATIONAL MANEUVER DESIGN

Characterizing the dynamical flow in the vicinity of a ballistic lunar transfer offers insight into trajectory design. To accommodate orbit determination errors, and small deterministic maneuvers along a trajectory, addressing the influence of perturbations on the solution is essential. The state transition matrix (STM) provides a linear approximation to the dynamical flow in the vicinity of the transfer. The STM is fundamental to all correction algorithms and is employed in the construction of previous transfers. The Singular Value Decomposition (SVD) is a function of the STM and aids in the classification of motion near the baseline. In contrast to an eigenvalue decomposition, SVD

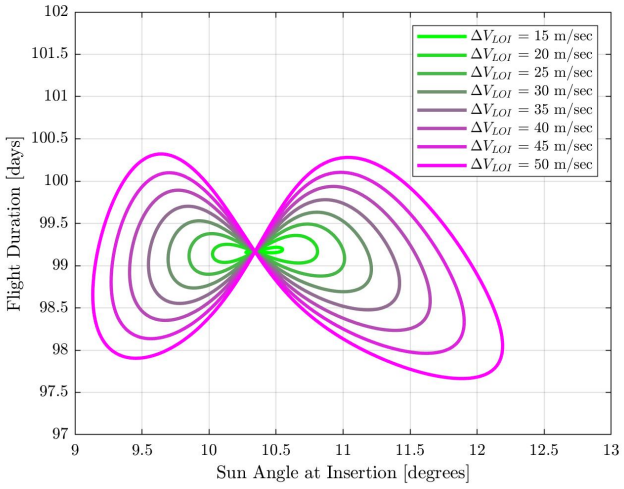

Figure 17. Evolution of flight duration as insertion Sun angle varies along multiple families of ballistic lunar transfers to a 9:2 NRHO

is applicable to both nonsingular and singular matrices. In the case where orbit determination errors are applied, the SVD enables separate linear predictions for the downstream position and velocity errors. Muralidharan and Howell the apply the stretching and restoring directions of the SVD for a stationkeeping framework.[16] Leveraging singular values along a ballistic lunar transfer supports a strategy to introduce deterministic maneuvers to the transfer design.

The singular values of a matrix predict the stretching and restoring motion localized to a baseline reference trajectory. The STM predicts the downstream influence of an initial perturbation. The STM is essentially a first-order, linear map, that is,

$$\delta\bar{x}(t) = \mathbf{\Phi}(t, t_0)\, \delta\bar{x}(t_0) \tag{11}$$

where $\mathbf{\Phi}(t, t_0)$ is the STM from some initial time t_0 to the final time t. The vectors $\delta\bar{x}(t_0)$ and $\delta\bar{x}(t)$ are the initial and final perturbations with respect to the states along the baseline. The elements of the STM are,

$$\mathbf{\Phi}(t, t_0) = \begin{bmatrix} \frac{\partial x}{\partial x_0} & \frac{\partial x}{\partial y_0} & \frac{\partial x}{\partial z_0} & \frac{\partial x}{\partial \dot{x}_0} & \frac{\partial x}{\partial \dot{y}_0} & \frac{\partial x}{\partial \dot{z}_0} \\ \frac{\partial y}{\partial x_0} & \frac{\partial y}{\partial y_0} & \frac{\partial y}{\partial z_0} & \frac{\partial y}{\partial \dot{x}_0} & \frac{\partial y}{\partial \dot{y}_0} & \frac{\partial y}{\partial \dot{z}_0} \\ \frac{\partial z}{\partial x_0} & \frac{\partial z}{\partial y_0} & \frac{\partial z}{\partial z_0} & \frac{\partial z}{\partial \dot{x}_0} & \frac{\partial z}{\partial \dot{y}_0} & \frac{\partial z}{\partial \dot{z}_0} \\ \frac{\partial \dot{x}}{\partial x_0} & \frac{\partial \dot{x}}{\partial y_0} & \frac{\partial \dot{x}}{\partial z_0} & \frac{\partial \dot{x}}{\partial \dot{x}_0} & \frac{\partial \dot{x}}{\partial \dot{y}_0} & \frac{\partial \dot{x}}{\partial \dot{z}_0} \\ \frac{\partial \dot{y}}{\partial x_0} & \frac{\partial \dot{y}}{\partial y_0} & \frac{\partial \dot{y}}{\partial z_0} & \frac{\partial \dot{y}}{\partial \dot{x}_0} & \frac{\partial \dot{y}}{\partial \dot{y}_0} & \frac{\partial \dot{y}}{\partial \dot{z}_0} \\ \frac{\partial \dot{z}}{\partial x_0} & \frac{\partial \dot{z}}{\partial y_0} & \frac{\partial \dot{z}}{\partial z_0} & \frac{\partial \dot{z}}{\partial \dot{x}_0} & \frac{\partial \dot{z}}{\partial \dot{y}_0} & \frac{\partial \dot{z}}{\partial \dot{z}_0} \end{bmatrix} \tag{12}$$

Each column of the STM describes the influence of one component of the initial state vector on the final vector perturbations. Likewise, each row of the STM reflects the impact on one component of the final state due to the initial perturbation vector. Thus, the STM is also written as,

$$\mathbf{\Phi}(t_f, t_0) = \begin{bmatrix} \mathbf{\Phi}_{r,r} & \mathbf{\Phi}_{r,v} \\ \mathbf{\Phi}_{v,r} & \mathbf{\Phi}_{v,v} \end{bmatrix} \tag{13}$$

where the values r and v refer to the position and velocity components, respectively. The terms $\mathbf{\Phi}_{i,j}$ represent the three-dimensional square submatrices of the full STM. The first subscript represents

the downstream variation, and the second subscript corresponds to the initial variation. Consider the term $\mathbf{\Phi}_{r,v}$, the submatrix represents the final change in position due to an initial perturbation in velocity, i.e., rows one through three and columns four through six of Equation (12). The term $\mathbf{\Phi}_{rv,v}$ considers the impact of an initial velocity perturbation on the entire downstream vector. A view of the local dynamics is obtained through either an eigendecomposition or SVD of the sub-matrices of the STM. An eigendecomposition is advantageous when the matrix is non-singular, and yields eigenvalues and the corresponding eigenvectors of the matrix. Where an eigendecomposition produces a matrix of eigenvectors and eigenvalues, the SVD factorizes a matrix into the product of three matrices,

$$\mathbf{\Phi}_{i,j} = \mathbf{U}\mathbf{\Sigma}\mathbf{V}^* \tag{14}$$

where $\mathbf{\Phi}_{i,j}$ is the STM, or a submatrix of the STM with dimensions m x n, the matrix $\mathbf{U}$ is defined with dimensions m x m and describes the stretching directions at the final state. The term $\mathbf{V}^*$ is the hermitian transpose of the matrix $\mathbf{V}$ with dimensions n x n, and represents the principal stretching directions at the initial time. The matrix $\mathbf{\Sigma}$, with dimensions of m x n, where the diagonal elements are the singular values (σ) of the matrix $\mathbf{\Phi}$.[16] Singular values are real, non-negative numbers, that represent the stretching or restoring motion near the baseline transfer. Singular values aid in the classification of ballistic lunar transfers.

Deterministic maneuvers aid in expanding launch window capabilities and extending the range of departure locations near the Earth. As ballistic lunar transfers are sensitive to variations in the departure Sun angle, adding a maneuver along the trajectory extends the range of usable launch epochs. This investigation assumes that a baseline trajectory is predetermined for the usable design, i.e., a single path to the Moon. Selecting a location to place a maneuver along the arc is nontrivial, as the goal is maximizing the range of departure epochs. A fixed maneuver magnitude constraint is located at time t along the baseline,

$$F_{\text{Det}} = \sqrt{\dot{\tilde{x}}_t^2 + \dot{\tilde{y}}_t^2 + \dot{\tilde{z}}_t^2} - \Delta V_{\text{Det}} - V_t \tag{15}$$

where F_{DET} is the deterministic maneuver constraint. In Equation (15) the quantities with subscript t represent the velocity components along the transfer at time t driving the propagation. The variable ΔV_{Det} is the maneuver magnitude allowed across a family of transfers, and V_t is the velocity of the ballistic lunar transfer at the time t. To better illustrate the purpose of the constraint, consider a sample scenario. A planar ballistic lunar transfer is selected, as illustrated in Figure 18. The transfer is defined by a flight duration of 100 days, and departs from a 150 km altitude LEO to arrive at a 100 km altitude LLO. The trajectory design is capable of allotting 20 m/sec of propellant for a maneuver to expand the launch window. To identify an effective location along the baseline trajectory to place the maneuver, a range of transfer families are constructed from the constraint in Equation (15). The baseline trajectory corresponds to a specific Sun angle at departure. For each day along the baseline, a family of transfers are constructed that target the maneuver location, with ΔV_{Det} = 20 m/sec. The range in departure Sun angle across a family corresponds to the launch window for placing a maneuver at that specific location along the ballistic lunar transfer. To illustrate one family, by placing the maneuver 63 days into the transfer (near apogee), the resultant range of solutions is depicted in Figure 19. The blue curves all depart from a 150 km altitude LEO with varying initial Sun angle. The yellow point indicates the insertion location onto the baseline trajectory. The red arc is the baseline arc, one that is preserved for all members of a given family. By incorporating a 20 m/sec maneuver at 63 days into the transfer, the range of initial epochs is 3.4 days. By repeating the process at one day intervals along the baseline, 100 families of orbits are constructed, and

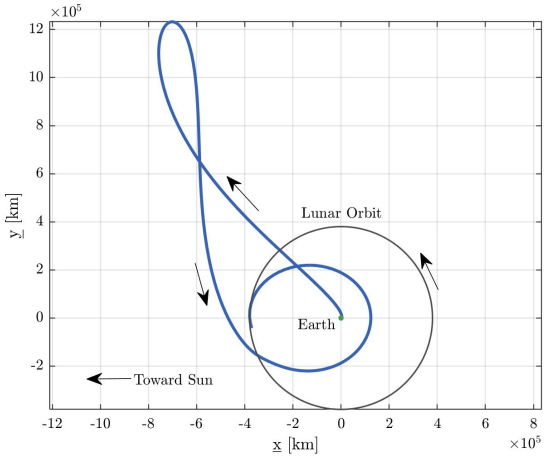

Figure 18. Sample ballistic lunar transfer, Sun-B_1 rotating frame centered at B_1

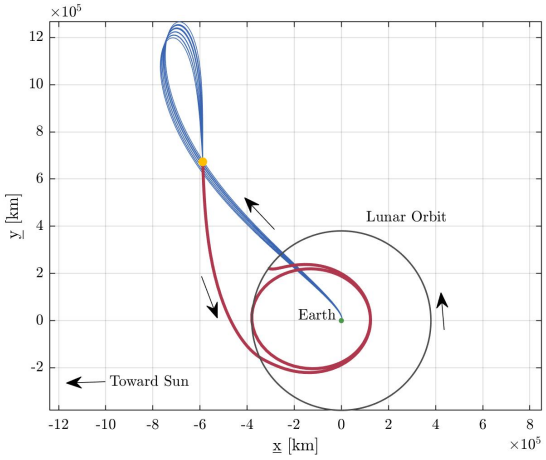

Figure 19. Family of trajectories arriving into the baseline ballistic lunar transfer, Sun-B_1 rotating frame centered at B_1

the launch window is compared across the possible maneuver placements. The variation in launch window across maneuver placement is illustrated in Figure 20. One disadvantage with the procedure to construct Figure 20 is the computational cost. Each family consists of a thousands separate transfers to the maneuver location that links with the ballistic lunar transfer. For every maneuver placement location added to the analysis, an additional one thousand transfers are produced to assess the launch window variation. To construct the curve represented in Figure 20, over one hundred thousand transfers were constructed. To reduce the computational costs, the singular values along the baseline transfer are assessed. A small maneuver along the baseline is the same as perturbation in velocity at some time t, i.e., the velocity components of the perturbation vector $\bar{x}(t)$. A linear prediction for a given perturbation is mapped by the STM. However, as illustrated by Figure 19, the maneuver occurs midway through the transfer. Therefore, the STM is created in reverse time, flowing from the end state at the Moon, back toward the Earth, written as $\mathbf{\Phi}(t_0, t)$. Such a matrix maps perturbations that occur at time t to the initial states departing from LEO. As the maneuver does not include a variation in position, the submatrix $\mathbf{\Phi}_{rv,v}$ from $\mathbf{\Phi}(t_0, t)$ is selected. Analyzing the

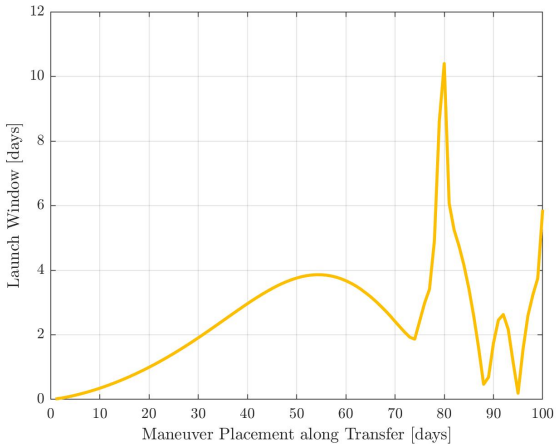

Figure 20. Evolution in launch window as maneuver location into the baseline varies

variation in the singular values as t varies along the transfer deliver insight into the stretching and restoring motion along the ballistic lunar transfer. Since the baseline is singular, the matrix $\mathbf{\Phi}_{rv,v}$ is 4x2, with two singular values of interest. Additionally, the singular values of the submatrices $\mathbf{\Phi}_{r,v}$ and $\mathbf{\Phi}_{v,v}$ represent physical quantities that predict the position and velocity perturbations, respectively. Return to the scenario where the maneuver is placed at 63 days into the transfer. Given the SVD from Equation (14) and the submatrix $\mathbf{\Phi}_{rv,v}$ from $\mathbf{\Phi}(0, 63)$, the two singular values are σ_1 = 1.87e6 ndim and σ_2 = 222 ndim, where ndim indicates nondimensional units. Both quantities are greater than one, thus, the prediction yields a deviation from the baseline. It is nontrivial to deduce information from a nondimensional quantity, e.g., identifying the particular singular value that relates to a variation in the launch window. Therefore, the singular values of $\mathbf{\Phi}_{r,v}$ and $\mathbf{\Phi}_{v,v}$ are,

$$\Sigma_{r,v}(0, 63) = \begin{bmatrix} 2.216e8 & 0 \\ 0 & 2.610e6 \end{bmatrix} \frac{km}{km/sec}$$

$$\Sigma_{v,v}(0, 63) = \begin{bmatrix} 1.87e6 & 0 \\ 0 & 2.22e2 \end{bmatrix}$$

By multiplying the maneuver magnitude by the singular value, an estimate for the downstream position and velocity perturbations are determined. With a 20 m/sec maneuver in the most stretching direction for position, the downstream variation in position is 4.32e6 km. The least stretching singular value yields a downstream perturbation of 5,000 km. The most stretching singular value predicts that the spacecraft departs the Earth-Moon system, while the least stretching direction in the $\widetilde{x}\widetilde{y}$-plane suggests an offset while still reaching the vicinity of the Earth in backwards time. The smallest singular value in the $\widetilde{x}\widetilde{y}$-plane provides an estimate for trajectories that deviate from the baseline while still passing in close proximity to Earth. An important point is that the spatial STM yields a restoring singular value. However, the restoring nature of perturbations in the $\widetilde{z}$ direction depict out-of-plane oscillations. To extend the analysis, the smallest singular values from the submatrix $\mathbf{\Phi}_{rv,v}$ are determined as $\mathbf{\Phi}(0, t)$ evolves from $t = t_0$ to t_f. The evolution of the minimum singular value in the $\widetilde{x}\widetilde{y}$-plane compared to the maneuver location is illustrated in Figure 21. Both Figure 20 and Figure 21 reflect the same general behavior, the same maneuver placement times along the baseline. Although the singular values of the submatrix $\mathbf{\Phi}_{rv,v}$ are nonphysical quantities, they depict ideal locations to place a maneuver to enable expansion of the launch window.

An advantage to the minimum singular value curve is a reduced computational load, as the analysis

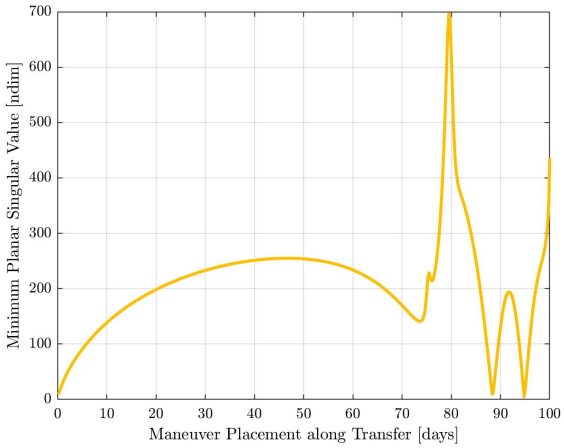

Figure 21. Evolution of singular values as the maneuver placement varies along the baseline transfer

is completed directly on the baseline trajectory. By leveraging techniques in dynamical systems theory, the data from Figure 21 is constructed by propagating 400 linear maps and performing matrix calculations. In practice, Figure 20 required many hours to construct the families necessary, while Figure 21 took a few seconds.

CONCLUDING REMARKS

Techniques in dynamical systems theory aid in the construction and characterization of ballistic lunar transfers. Low-energy transfers offer propellant efficient paths to various locations in cislunar space. The 9:2 synodic resonant NRHO is notable as the Gateway program continues to develop. A family of 9:2 NRHOs in the BCR4BP is constructed, and periapse Poincaré maps are incorporated to identify end-to-end ballistic lunar transfers. The analyses focused on three separate stages of a ballistic lunar transfer. By fixing the injection maneuver for the transfer, a family of solutions with various LOI costs and flight durations is constructed. With proper selection of an initial guess, a family of transfers that leverage an outbound lunar flyby are achievable. Similarly, by fixing the lunar insertion cost, a comparison is made between the TLI costs and transfer durations. The third phase examined placing a maneuver along the coast arc to extend the viable departure epochs. Through the analysis, linear mapping methods aid in the characterization of ballistic lunar transfers. A strategy to construct families of ballistic lunar transfers for low-energy trajectory design is introduced; the same approach was also leveraged to use small maneuvers to expand the launch window.

ACKNOWLEDGMENTS

The authors would like to thank the School of Aeronautics and Astronautics at Purdue University, and the Rune and Barbara Eliasen Visualization Laboratory for facilities and financial support. The authors would also like to thank the members of the Purdue Multi-Body Dynamics Research Group for informative discussions. This work was completed under NSF Grant No. 10001485. The authors very much appreciate the support.

REFERENCES

[1] R. M. Smith, N. Merancy, and J. Krezel, "Exploration Missions 1, 2, and Beyond: First Steps Toward a Sustainable Human Presence at the Moon," *2019 IEEE Aerospace Conference*, Vol. 2019-, IEEE, 2019, pp. 1–12.

[2] N. L. Parrish, E. Kayser, S. Udupa, J. S. Parker, B. W. Cheetham, and D. C. Davis, "Ballistic Lunar Transfers to Near Rectilinear Halo Orbit: Operational Considerations," *AIAA Scitech 2020 Forum*.

[3] S. Campagnola, J. Hernando-Ayuso, K. Kakihara, Y. Kawabata, T. Chikazawa, R. Funase, N. Ozaki, N. Baresi, T. Hashimoto, Y. Kawakatsu, T. Ikenaga, K. Oguri, and K. Oshima, "Mission Analysis for the EM-1 CubeSats EQUULEUS and OMOTENASHI," *IEEE Aerospace and Electronic Systems Magazine*, Vol. 34, 04 2019, pp. 38–44, 10.1109/MAES.2019.2916291.

[4] V. G. Szebehely, *Theory of Orbits: The Restricted Problem of Three Bodies*. New York: Academic Press, 1967.

[5] K. K. Boudad, "Disposal Dynamics from the Vicinity of Near Rectilinear Halo Orbits in the Earth-Moon-Sun System," 2018. M.S. Thesis, Purdue University, West Lafayette, Indiana.

[6] S. T. Scheuerle, "Construction of Ballistic Lunar Transfers in the Earth-Moon-Sun System," 2021. M.S. Thesis, Purdue University, West Lafayette, Indiana.

[7] J. S. Parker and G. H. Born, "Modeling a Low-Energy Ballistic Lunar Transfer Using Dynamical Systems Theory," Vol. 45, 2008, pp. 1269–1281.

[8] B. P. McCarthy and K. C. Howell, "Cislunar Transfer Design Exploiting Periodic and Quasi-Periodic Orbital Structures in the Four-Body Problem," *71th International Astronautical Congress*, 2020.

[9] C. Warner, "NASA's lunar outpost will extend human presence in deep space," *NASA TV [online journal]*, 2018.

[10] E. M. Zimovan-Spreen, K. C. Howell, and D. C. Davis, "Near Rectilinear Halo Orbits and Their Application in Cis-lunar Space," *3rd International Academy of Astronautics Conference on Dynamics and Control of Space Systems*, 2017.

[11] K. K. Boudad, K. C. Howell, and D. C. Davis, "Dynamics of Synodic Resonant Near Rectilinear Halo Orbits in the Bicircular Four-body Problem," *Advances in Space Research*, Vol. 66, No. 9, 2020, pp. 2194–2214, https://doi.org/10.1016/j.asr.2020.07.044.

[12] J. S. Parker, "Targeting Low-Energy Ballistic Lunar Transfers," *The Journal of the Astronautical Sciences*, Vol. 58, No. 3, 2011, pp. 311–334.

[13] D. C. Davis and K. C. Howell, "Characterization of Trajectories Near the Smaller Primary in the Restricted Problem for Applications," *Journal of Guidance, Control, and Dynamics*, Vol. 35, No. 1, 2012, pp. 116–128.

[14] A. F. Haapala and K. C. Howell, "Representations of higher-dimensional Poincaré maps with applications to spacecraft trajectory design," *Acta Astronautica*, Vol. 96, Mar. 2014, pp. 23–41, 10.1016/j.actaastro.2013.11.019.

[15] S. T. Scheuerle, B. P. McCarthy, and K. C. Howell, "Construction of Ballistic Lunar Transfers Leveraging Dynamical Systems Techniques," *AIAA/AAS Astrodynamics Specialist Conference*, 2020.

[16] V. Muralidharan and K. C. Howell, "Stationkeeping in Earth-Moon Near Rectilinear Halo Orbits," *AAS/AIAA Astrodynamics Specialist Conference*, 2020.